



Characterization and solderability of cold sprayed Sn–Cu coatings on Al and Cu substrates

J.F. Li ^{a,*}, P.A. Agyakwa ^a, C.M. Johnson ^a, D. Zhang ^b, T. Hussain ^b, D.G. McCartney ^b

^a Department of Electrical and Electronic Engineering, The University of Nottingham, University Park, Nottingham NG7 2RD, United Kingdom

^b Department of Mechanical, Materials and Manufacturing Engineering, The University of Nottingham, University Park, Nottingham NG7 2RD, United Kingdom

ARTICLE INFO

Article history:

Received 5 August 2009

Accepted in revised form 9 September 2009

Available online 17 September 2009

Keywords:

Roughness

Photoelectron spectroscopy

Transmission electron microscopy (TEM)

Tin

Tin oxide

Cold spraying

ABSTRACT

Cold sprayed Sn–Cu coatings approximately 40 and 25 μm in average thickness were deposited on aluminium and direct bonded copper (DBC) substrates respectively. Both a statistical analysis of coating thickness and a roughness analysis of the coating/substrate interface and the coating surface were carried out for the as-sprayed coatings using scanning electron microscope images. The results obtained can be related to substrate types and spraying conditions. Tin oxide on the surfaces of the as-sprayed coatings was revealed by employing X-ray photoelectron spectroscopy analyses and transmission electron microscopy. It came from an oxide shell around feedstock powder particles and was only locally broken down during cold spraying. Although the tin oxide inhibited fluxless soldering, flux-supported reflow of cold sprayed Sn on the DBC substrate produced Cu/Sn/Cu solder joints that were acceptable for application in electronic packaging and interconnects. In general, measures which can avoid or remove the tin oxide are needed to achieve improved solder joints using cold sprayed Sn coatings as the solder layers.

© 2009 Elsevier B.V. All rights reserved.

1. Introduction

Cold gas dynamic spraying, commonly referred to as cold spray, was developed in the mid 1980s at the Institute of Theoretical and Applied Mechanics of the Siberian Division of the Russian Academy of Science in Novosibirsk [1,2]. During cold spray, powder particles, usually in the size range of 1 to 50 μm , are accelerated through a de Laval type of converging–diverging nozzle by a supersonic gas flow. Typically particle speeds of 300 to 1200 m/s are attained and the powder particles are directed to impact on a substrate or previously deposited powder to form a coherent coating. Heated air or nitrogen may be used as the accelerating gas but the best quality of coatings is generally achieved by using helium at room, or slightly elevated, temperature [2,3]. Al and Cu coatings deposited by cold spray have been the most extensively investigated to date. Studies have included optimization of the spraying process, the bonding mechanism, microstructure formation and the thermal stability of the deposits [3–9]. A number of other metallic materials have also been reported to be successfully deposited by cold spray to produce coatings, including Sn, Al–Sn and Cu–Sn as examples relevant to the present work [10–14].

Cold sprayed coatings are reported to have relatively low porosity and a low oxygen or oxide content [14,15]. As a result, cold spray has been investigated as a method to produce solderable surfaces on

materials with poor wettability (e.g. heat sinks, such as Cu on Al) and to deposit brazing and soldering alloys for applications in electronic packaging and interconnects [15,16]. For example, a cold sprayed Cu coating on a heat sink made of Al as a base layer has been successful as a solderable surface for the Sn- or Cu-plated area of electronic devices [15]. In this case, the high kinetic energy of the Cu particles was sufficient to break up the oxide film on the aluminium surface. For similar electronic applications, cold sprayed Al coatings might also be used as bonding layers, e.g. onto a hard and brittle Al_2O_3 substrate, for depositing other top layers, such as Cu and Sn, using another coating/film process [15].

Another interesting effort in the field of cold spray was the deposition of conducting layers onto plastics [16]. By controlling the spraying process conditions, it was possible to deposit Cu onto PA 66 (nylon 6/6), but the bond strength between the Cu deposit and the substrate appeared to be rather low.

Cold spray has been investigated for depositing Sn-based solder alloy layers although substrate types were not reported [15]. Also the effects of substrate temperature and gun transverse speed on the formation mechanism of cold sprayed Sn coatings were also systematically studied by Legoux et al. [11]. Although a deposition efficiency of less than 5% was reported for Sn coatings on a steel substrate, scanning electron microscopy images of the polished cross sections indicate that a continuous solder layer with a thickness of 20 to 30 μm and a surface roughness, R_a , of 1–20 μm could be achieved, see Fig. 13 in [11].

In addition, cold spray was used to deposit Zn–Al–Si brazing alloys for joining Al or Al-based alloys [17]. In this case, the cold spray process

* Corresponding author.

E-mail address: Jian.Li@nottingham.ac.uk (J.F. Li).

used hot air with temperatures from 100 to 300 °C as the accelerating gas [18]. Deposited monolithic or composite coatings included both brazing materials and corrosion protection materials and can be used for brazing aluminium fins to plates and tubes of heat exchangers in a single stage.

The purpose of the present work was to assess the potential for employing cold sprayed Sn–Cu coatings as solder layers. The main objective of this paper is to systematically characterize the cold sprayed Sn–Cu coatings and to clarify the challenges that need to be addressed before cold spray can be reliably used to pre-deposit Sn-based layers for effective soldering in electronic packaging and interconnects. (As the copper content was low the deposits will be referred to as Sn coatings throughout the rest of the paper.)

Therefore, cold sprayed Sn coatings approximately of 40 and 25 μm in thickness were deposited on aluminium and direct bonded copper (DBC) substrates, respectively. We report here the results including: (i) statistical analysis of thickness and roughness parameters of surface and coating/substrate interface for the as-sprayed coatings based on scanning electron microscopy (SEM) images; (ii) identification of surface oxides on the as-sprayed coatings using X-ray photoelectron spectroscopy (XPS) and transmission electronic microscopy (TEM); and (iii) results of both flux and fluxless soldering trials intended to join the aluminium and DBC using the cold sprayed Sn coatings as the solder layers.

2. Experimental procedure

2.1. Materials

Pure Sn powder of nominal size range $-30 + 5 \mu\text{m}$ mechanically blended with 5 wt.% of $-30 + 5 \mu\text{m}$ pure Cu powder was used as feedstock for cold spray. 5 wt.% Cu was added into the feedstock because Sn-based solders are generally alloyed with other metals to suppress the well known “tin pest” at temperatures below 13 °C [19]. A SEM image of the particles present in the blended powders is shown in Fig. 1(a). They are seen to have a spherical morphology which is typical of metallic powders prepared using an inert gas atomizing process. The corresponding particle size distribution obtained using image analysis method from SEM micrographs is shown in Fig. 1(b), where the powder particles were approximated as ideal spheres and the particle size of 21.3 μm corresponds to the cumulative volume fraction of 0.5; what is commonly termed the d_{50} value of the powder.

Cu and Al are both used extensively as contact metallizations and/or materials for thermal management in electronic assemblies and systems [20] and were thus selected as materials for the substrates used in these studies. The Al substrate was commercially available 1 mm thick 99.99% Al sheet with a microhardness $Hv_{0.2\text{kg}}$ of 28 kgfmm^{-2} . Prior to cold spraying, it had been cut into $100 \times 12 \times 1 \text{ mm}$ coupons. The Cu substrate was direct bonded copper (DBC) that is widely used in power electronics for supporting semiconductor devices. In cross-section, it consists of two layers of 0.3 mm thick Cu (with a microhardness $Hv_{0.2\text{kg}}$ of 75 kgfmm^{-2}) sandwiching a layer of 0.4 mm thick alumina. Before cold spraying, it had been cut into the coupons of $100 \times 12 \times 1 \text{ mm}$ in size. The cut Al and Cu coupons were cleaned using isopropyl alcohol, without the need of any further surface preparation.

2.2. Cold spray deposition

Cold spray was carried out at the University of Nottingham using an in-house constructed cold-gas spraying system, which is described in detail elsewhere [16]. A schematic diagram of the spraying system is shown in Fig. 2, where room temperature helium was employed as the gas for both particle acceleration and powder feeding. The powder feedstock was delivered into the gun chamber using a Praxair Model 1264 high pressure powder feeder.

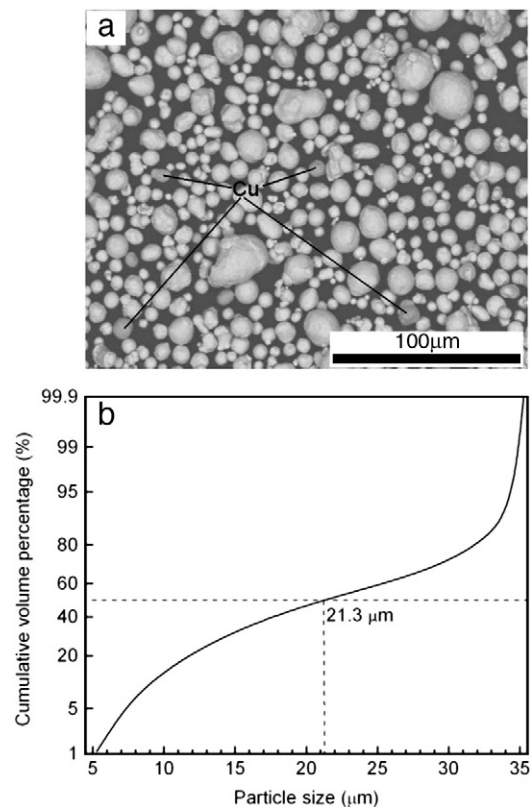


Fig. 1. (a) SEM image and (b) cumulative particle size distribution plotted on a normal probability co-ordinate of the mechanically blended 95 wt.% Sn plus 5 wt.% Cu powder feedstock.

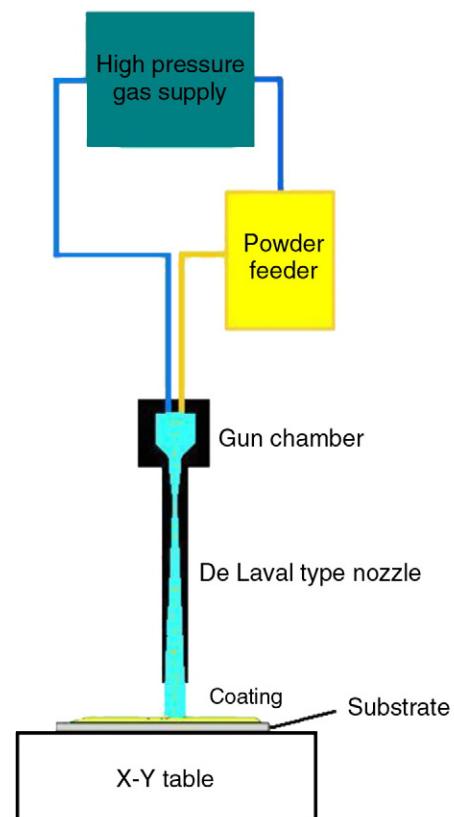


Fig. 2. Schematic diagram of the cold spray system.

Table 1

Sample codes and the main processing parameters of the cold sprayed Sn–Cu coatings.

Sample code	AA1	AA2	AC1
Substrate	Al	Al	DBC
He pressure (MPa)	1.0	2.0	1.0
Powder feed rate (g/min)	15	15	15
Standoff distance (mm)	20	20	20
Gun traverse speed (mm/s)	100	100	100

Following initial trials, two sets of processing parameters were employed to spray the feedstock of blended Sn–Cu powder particles. Sample codes and the corresponding processing parameters are listed in Table 1. In all cases, the pressure of the powder carrier gas was 0.1 MPa above that of the main accelerating gas. All three coatings were produced in a single pass because multiple passes were found to lead to de-bonding of the coatings from the substrates. The stand alone de-bonded coatings produced by two passes were somewhat thicker (100–150 μm) than the coatings prepared using a single spraying pass which were typically 25–40 μm thick.

2.3. Soldering trials

As reported below, the coating coded AA2 was discontinuous. Thus only the as-sprayed AA1 and AC1 coatings were cut into pieces of $12 \times 10 \times 1$ mm and $15 \times 12 \times 1$ mm respectively for soldering experiments. The soldering experiments were carried out using the sample geometries shown in Fig. 3. Because of the deformation of the Al substrate caused during cutting, a layer of 50 μm eutectic Sn–Ag foil was inserted in the middle to improve the gap filling for the AA1 coating, Fig. 3(a). Before the soldering processes, all samples were ultrasonically cleaned using isopropyl alcohol (IPA), rinsed using acetone and deionised water. For purposes of comparison, three reflow processes termed RP1, RP2 and RP3 were employed and are listed in Table 2. They were used for both the Al/Sn–SnAg–Sn/Al (AA1) and DBC/Sn–Sn/DBC (AC1) systems.

Of the three reflow processes listed in Table 2, RP1 and RP2 are typical of a fluxless soldering process that might be applied in the assembly of power electronic modules either for die or substrate mount down. Such processes typically involve the use of solder foil pre-forms normally between 100 and 400 μm in thickness. Forming gas is used to clean the surfaces and a vacuum is used to reduce voiding. This process is preferred for making large area (>100 mm^2) bonds. Surface abrading used in RP2 is to see whether this could effectively remove surface oxide on the coatings. RP3 is typical of the fluxed solder reflow process that is widely used in electronics

assembly. Here a pre-fluxed solder paste is employed and reflow takes place in an ambient air environment.

2.4. Coating and solder joint characterization using scanning electron microscopy (SEM)

A JEOL 6400 SEM was used to examine as-sprayed coating top surfaces and cross-sections of coating microstructures using secondary electron (SE) and backscattered electron (BSE) imaging.

Metallographic cross-sections of the coatings were prepared for thickness and roughness measurements using the following procedure. The coating samples were first cut into pieces approximately $15 \times 5 \times 1$ mm and then mounted in epoxy resin that was cured at room temperature for 24h. The mounted samples were then successively ground with 400, 800, 1000, 1200 and 2400 grit SiC papers and finally polished using diamond slurries of 3 μm and 1 μm for 10 min and 5 min, respectively.

The image analysis method used to extract the original substrate/surface, coating/surface and coating/substrate interfacial profiles from the cross-sectional SEM images utilized the Image Processing Toolbox Version 5.0.0 of MATLAB R14SP2 (Mathworks) and is shown schematically in Fig. 4. For each sample, three to five images at a resolution of 512×416 pixels and an image size of $1175 \times 940 \mu\text{m}$ were used and the obtained data were merged together. Fig. 4(a) shows a SEM image and Fig. 4(b) reveals the extracted profiles. The thickness of a coating sample can be expressed, in principle, as a function of location x along the coating by:

$$t(x) = z_t(x) - z_b(x), \quad x \in [0, L_0] \quad (1)$$

where $t(x)$ is the thickness, L_0 is the cross-sectional length of the profiles, $z_t(x)$ and $z_b(x)$ are the vertical coordinates of the profiles of the coating surface and the coating/substrate interface, respectively, see Fig. 4(c). The captured digital SEM images were used to generate data sets and so Eq. (1) takes on a discrete form:

$$t_i = z_t(x_i) - z_b(x_i), \quad i = 1, 2, \dots, n \quad (2)$$

where n is the total number of data points. Then the mean, standard deviation, minimum and maximum values of the thickness data can be calculated as detailed in [21,22]. In addition, the cumulative probability for the resulting thickness data, $f(t_j)$, could be obtained from placing the data in ascending order and letting

$$f(t_j) = \frac{j-0.5}{n}, \quad j = 1, 2, \dots, n \quad (3)$$

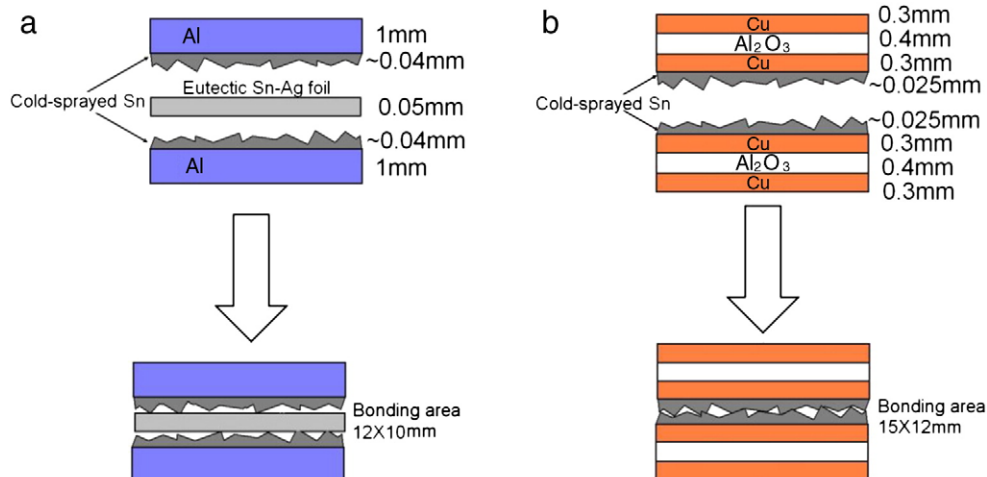


Fig. 3. Schematic sample geometries for the soldering experiments: (a) Al/Sn–SnAg–Sn/Al (AA1) and (b) DBC/Sn–Sn/DBC (AC1) systems.

Table 2
Reflow parameters of the three soldering trials.

Soldering trial	Surface preparation	Reflow temperature and environment profiles
RP1	None	<ol style="list-style-type: none"> 1. Pre-heated up to 200 °C and evacuated below 5 mbar for 3 min 2. Held at 200 °C and purged with 2% H₂98%N₂ forming gas (450 L/h at 1.5 bar) for 10 min 3. Heated up to 260 °C and evacuated below 5 mbar for 3 min 4. Held at 260 °C under nitrogen flow of 450 L/h at 1.5 bar for 5 min 5. Cooled down to room temperature within 5 min
RP2	As-sprayed surfaces of the Sn coatings were manually abraded using grade 4000 SiC paper for 10 s	Identical to those above for soldering trial RP1
RP3	As-sprayed surfaces of the Sn coatings were covered with a layer of mild active resin flux	<ol style="list-style-type: none"> 1. Pre-heated up to 200 °C under air for 3 min 2. Further heated up to 260 °C under air over 2 min 3. Held at 260 °C under air for 5 min 4. Cooled down to room temperature naturally

where j is the j th order in ascending thickness data [21]. If some values of thickness t_j were identical in the ascending order, only the one corresponding to the largest cumulative probability was retained and the others were deleted in the final curve of the cumulative probability curves.

For a surface or interfacial profile (see Fig. 4(c)), the roughness parameters, R_p and R_v are respectively the distances of the highest peak and lowest valley to the central line, and roughness parameter R_a is defined as [23]:

$$R_a = \frac{1}{n} \sum_{i=1}^n |z(x_i) - \overline{z(x_i)}| \quad (4)$$

where $z(x_i)$ ($i = 1, 2, \dots, n$) is the vertical coordinate of the profile as a function of location x_i . The average vertical coordinate:

$$\overline{z(x_i)} = \frac{1}{n} \sum_{i=1}^n z(x_i). \quad (5)$$

Here the roughness parameters were calculated from the entire cross-sectional profile extracted from the SEM images. This results in a sampling length shorter than, and an accuracy similar to, the geometrical product specifications established by the ISO technical committee detailed in [23].

After the reflow processes, the interfacial microstructures of the resulting samples were characterized using the same procedures for sample preparation and SEM observation as those used for the as-sprayed Sn coatings. The intermetallic compounds (IMCs) formed between Sn and Cu after the reflow processes were identified with the aid of energy-dispersive X-ray spectroscopy (EDXS) using an Oxford Instruments ISIS microanalysis system fitted on the SEM.

2.5. Coating characterization by XPS and TEM

XPS was employed to analyze the chemical state of Sn atoms at the surfaces of the as-received Sn powder particles and the as-sprayed coatings AA1 and AC1. The XPS spectra were collected using the Kratos AXIS ULTRA with a mono-chromated Al K α X-ray source (1486.6 eV) typically operated at 15 mA emission current and 10 kV anode potential. The XPS spectra collected were calibrated using the corresponding C 1 s aliphatic peaks. TEM was used to further examine

the phases on the coating surface. This was done using a JEOL 2000 FX TEM, fitted with an Oxford Instruments ISIS EDXS microanalysis system. Because of very rough surfaces and brittle nature of the coatings, a few coating particles were obtained using a knife of stainless steel to scratch the surface of coating AC1 and dispersed onto extremely thin carbon film fixed on copper mesh for the TEM analysis.

3. Results

3.1. As-sprayed Sn coatings

3.1.1. Microstructure

Fig. 5 presents the SEM images showing the microstructures of the as-sprayed coatings. Despite a few small pores, all the coatings are seen to have porosity values lower than ~1%. Cu particles are occasionally visible, embedded within the Sn, and the Cu contents are obviously lower than the 5 wt.% in the feedstock powder (Fig. 5(a) to (c)). The as-sprayed surfaces of the coatings exhibit a cellular

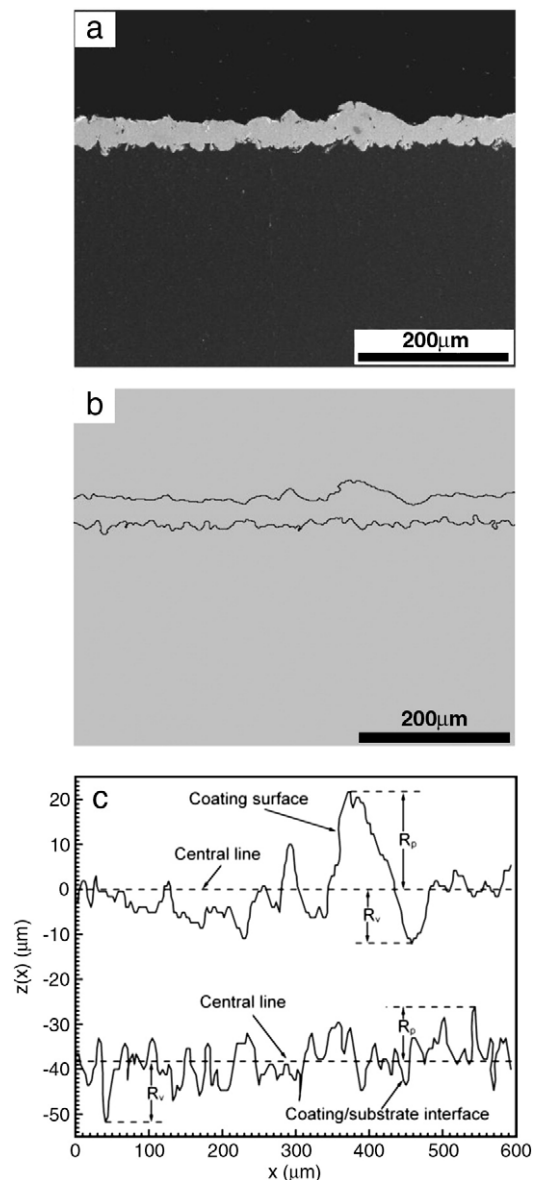


Fig. 4. Schematic illustration of the method for calculating the roughness parameter from an original cross-sectional SEM image: (a) SEM image taken from the as-sprayed coating AA1; (b) the extracted profiles of both the coating surface and the coating/substrate interface; and (c) the roughness parameters R_p and R_v and the quantities used to calculate the roughness parameter R_a .

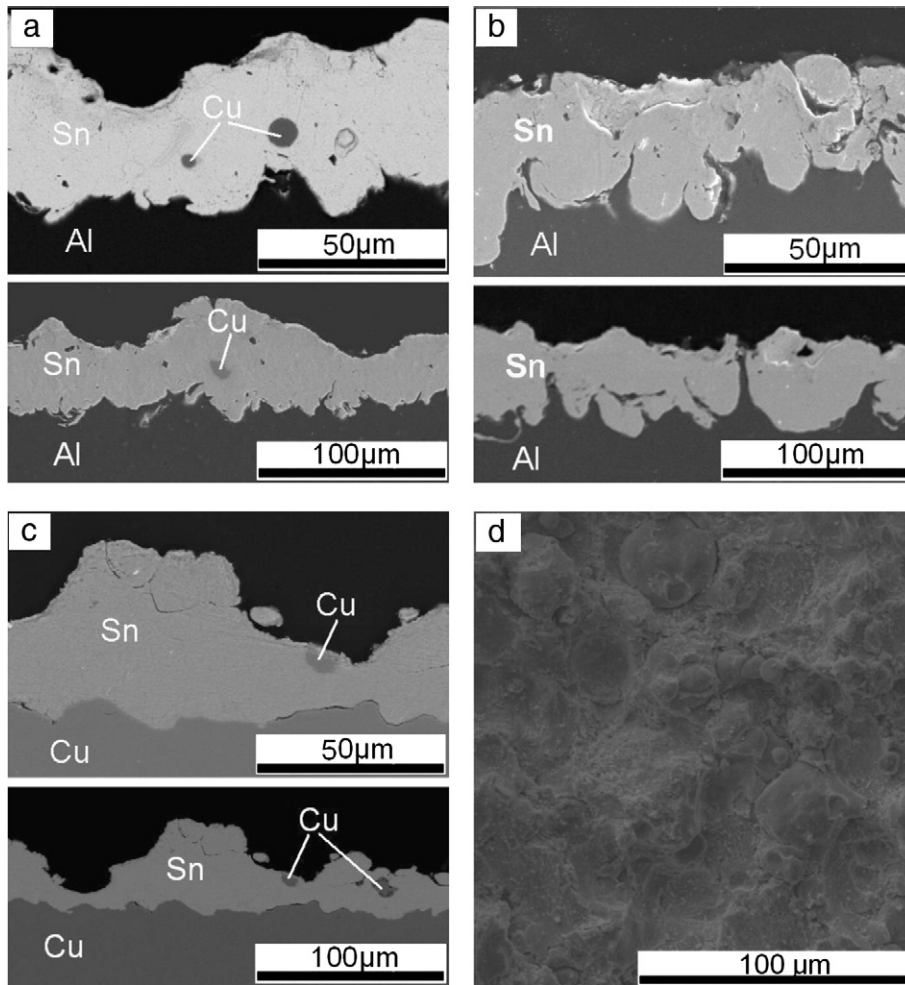


Fig. 5. SEM images of the three as-sprayed Sn coatings: (a) AA1, polished cross section; (b) AA2, polished cross section; (c) AC1, polished cross section; and (d) AC1, as-sprayed surface.

morphology of particles that were impacted and bonded on the previously deposited particles (Fig. 5d). However, the flattening of the particles was rather limited.

Using the lower pressure (1.0 MPa) for the helium gas, continuous coatings AA1 and AC1 were achieved on both the Al and Cu substrates. Both the surface and coating/substrate interface profiles are rather rough, and the surface profiles are apparently rougher than the coating/substrate interface profiles (Fig. 5(a) and (c)). Comparing the coatings on the two substrates, the coating AA1 on the Al substrate is thicker, and has a less rough surface but more irregular coating/substrate interface than the coating AC1 on Cu substrate.

Using a higher pressure (2.0 MPa) for the helium gas, the majority of the Sn particles were found to penetrate into the Al substrate more significantly than with coating AA1 and the resulting coating AA2 was discontinuous (Fig. 5(b)). The coating/substrate interface became rougher and has similar irregularity to the surface.

No metallurgical interfacial reaction (involving formation of a new phase) was detected and hence a solid state bond has apparently formed between the coatings and the substrates. Craters that were produced due to the high-velocity impact of the initial Sn particles had enhanced the bonding of the deformed Sn particles to the substrates

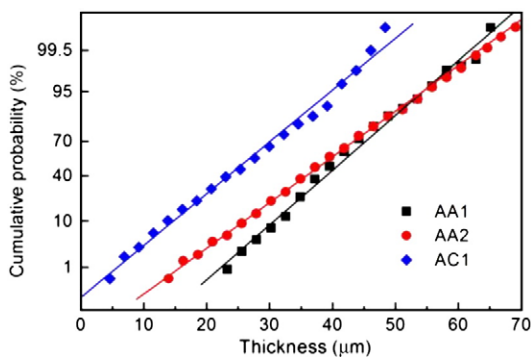


Fig. 6. Cumulative probability curves of the thickness variations of the three as-sprayed coatings on normal probability coordinates.

Table 3

Results of thickness measurement and surface roughness analysis of the as-sprayed Sn-Cu coatings.

Sample code		AA1	AA2	AC1
Coating thickness	Mean (µm)	39.7	35.7	25.1
	S.D. (µm)	7.8	11.4	9.1
	t_{min} (µm)	16.1	0.0	4.6
	t_{max} (µm)	64.5	69.8	48.8
Coating surface	R_a (µm)	5.2	5.7	6.9
	R_p (µm)	23.8	21.9	24.5
	R_v (µm)	20.1	15.4	17.5
	R_z (µm)	4.9	6.3	2.6
Coating/substrate interface	R_p (µm)	18.1	20.1	8.0
	R_v (µm)	15.6	21.8	9.6
	R_a (µm)	2.3	2.3	1.3
	R_z (µm)	7.8	7.8	3.6
Original substrate surface	R_p (µm)	7.8	7.8	3.6
	R_v (µm)	9.1	9.1	2.9

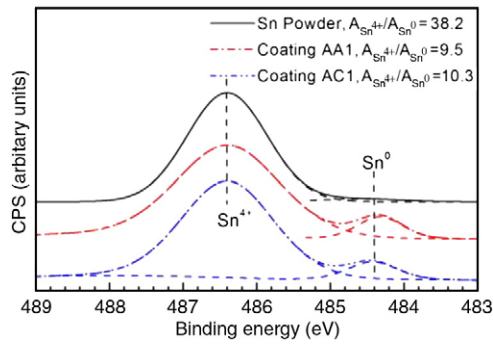


Fig. 7. Sn 3d XPS spectra for the as-received Sn powder and the as-sprayed coatings AA1 and AC1. $A_{\text{Sn}^{4+}}^+$ and $A_{\text{Sn}^0}^0$ represent the areas of the peaks corresponding to Sn^{4+} and Sn^0 states.

and produced the irregular profiles of the coating/substrate interfaces (Fig. 5).

3.1.2. Statistical analysis of coating thickness

The data obtained from the coating thickness measurements using image analysis were analyzed as described in this section. Fig. 6 presents cumulative probability curves of thicknesses variations of the three as-sprayed coatings plotted on normal probability coordinates, where the vertical axis is in the probability scale representing the inverse of a cumulative Gaussian distribution as expressed as:

$$\Phi^{-1}[F(t)] = -\frac{\mu}{\sigma} + \frac{1}{\sigma}t \quad (7)$$

where μ is the mean, σ is the standard deviation and $F(t)$ is the cumulative Gaussian function:

$$F(t) = \frac{1}{\sigma\sqrt{2\pi}} \int_{-\infty}^t \exp\left(-\frac{t-\mu}{2\sigma^2}\right) dt. \quad (8)$$

Therefore, for data following an ideal normal distribution, the cumulative probability curve would be a straight line on the normal probability coordinates. As shown in Fig. 6, this is the case for the thickness variations of all the three as-sprayed coatings.

Among the three coatings, a lower slope indicates that the thickness of coating AA2 on Al substrate produced using a higher pressure (2.0 MPa) for the He gas shows more variability than that of the coating AA1 on the Al substrate which was produced with a lower helium gas pressure (1.0 MPa). The coating AC1 on Cu substrate is seen to be thinner than, but has uniformity similar to, that of coating AA1. The latter can be seen from their cumulative probability curves which are approximately parallel to one another.

The characteristic parameters of the normal distribution, including the mean and standard deviation, together with the minimum and maximum values of the thickness of the three as-sprayed coatings are listed in Table 3. It can be further seen that the average thickness, i.e. the mean of coating AA2 is slightly less than that of coating AA1. All the three coatings have maximum thicknesses that are obviously greater than the diameter of the largest particle in the feedstock powder. In addition, based on the known powder feed rate, gun traverse speed and step width, the deposition efficiencies for production of the three coatings were calculated from the average thicknesses listed in Table 3. In this calculation, pores within the coatings were ignored and the density of Sn was taken as 7287 kgm^{-3} for both the powder particles and the coatings. The calculated deposition efficiencies are 46%, 42% and 29% for the coatings AA1, AA2 and AC1, respectively.

3.1.3. Roughness analysis

The results of the roughness measurements for the coating surface, the coating/substrate interface and the original substrate surface of

the three coatings are also listed in Table 3. Compared with the original substrate surfaces, the coating/substrate interfaces are seen to be coarsened with significantly increased roughness parameters. This is because the interfaces consist of craters produced by high-velocity impacting Sn particles during the initial deposition stage. It is thus easily understood that the coating/Al interfaces are more irregular than the coating/Cu interface because the Al substrate is somewhat softer than the Cu substrate. It is interesting to note that the roughness parameters of the coating/Al interface are increased when the pressure of the helium gas was doubled.

3.1.4. Surface analysis

XPS spectra can be used to analyze the chemical states of a few layers of atoms at the surface of a material. As shown in Fig. 7, obtained from Sn powder and coating top surfaces, the weak peaks at 484.4 eV for the Sn 3d XPS binding energy correspond to the Sn atoms in the form of metallic tin (Sn^0), while the dominant peaks at 484.4 eV correspond to those of tin oxide (Sn^{4+}) [24]. From the ratio of peak area for Sn^{4+} to that for Sn^0 , it can be seen that the surfaces of the as-received Sn powder particles are covered with an oxide shell. This layer of oxide might be formed during the manufacturing process or transportation and storage of the Sn powder. After cold spraying, the oxide shell had apparently been broken down locally to expose metallic Sn atoms on the coating surfaces, as reflected by the increased intensities of the XPS peaks for Sn^0 . However, the exposure of fresh Sn atoms is limited and the as-sprayed coating surfaces were still predominately covered by the tin oxide.

Fig. 8 displays the results of TEM analysis of the particles removed from the top surface of coating AC1. Fig. 8(a) and (d) are TEM images of separate polycrystalline particles. Fig. 8(b) and (e) are the respective selected area electron diffraction (ED) patterns. The discrete spots on Fig. 8(b) correspond to the interplanar spacings which are consistent with those of SnO_2 . The rings drawn on Fig. 8(b) are the patterns which would be produced by a polycrystalline SnO_2 sample. In Fig. 8(e), a number of discrete diffraction spots are visible. Also drawn on Fig. 8(e) are the rings which would be produced by a polycrystalline Sn sample and also a [331] zone axis pattern for Sn. Therefore, the corresponding selected areas in Fig. 8(a) and (d) are SnO_2 and Sn respectively. This is confirmed by the EDXS spectra in Fig. 8(c) and (f), where a more pronounced oxygen peak is seen in Fig. 8(c). Note that the minimum electron beam spot size achievable for the EDXS analysis was approximately 200 nm, and some Cu came from the supporting Cu mesh for the sample. Because of the destructive nature of TEM sample preparation, it is difficult to obtain the images directly reflecting the distribution of the SnO_2 layer on the coating surface. Nevertheless, from the size of the SnO_2 grains, it can be reasonably deduced that the oxide shell on the as-received Sn powder particles, and hence the oxide layer covering most surfaces of the as-sprayed coatings, is a few to ten nm in thickness.

3.2. Soldering

3.2.1. Sn coating on Al substrate – coating AA1

After reflow process RP1 under nitrogen, the Sn coating was still mechanically bonded to the Al substrate. However, the coating failed to bond to the eutectic SnAg solder foil between the substrates (see Fig. 3 for schematic of the process). Fig. 9(a) shows that the surface of the coating still has a roughness profile similar to the as-sprayed surface. These reflow results indicate that the thin layer of tin oxide on the coating surface is very tenacious. Only a very small part of the molten Sn could have flowed out of the locally fresh surface into the SnAg solder to slightly reduce the average thickness of the coating from 40 to 38 μm .

When the as-sprayed surface of the Sn coating was first manually abraded using grade 4000 SiC paper for 10 s, the Sn coating on the two sides of the Al/Sn–SnAg–Sn/Al sample could be partially joined to the

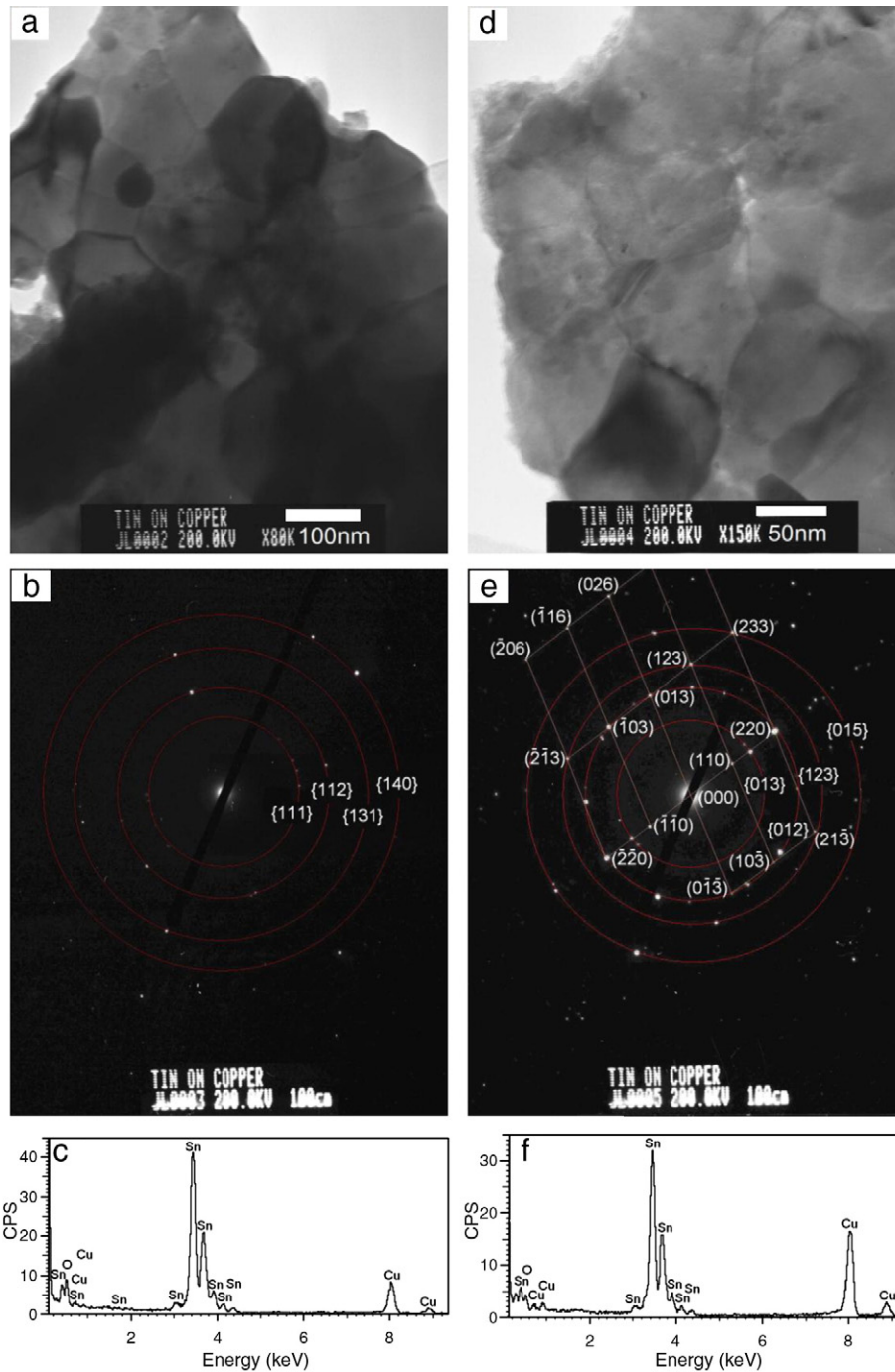


Fig. 8. TEM results of particles removed from the surface of coating AC1: (a) TEM image of one Sn particle; (b) selected area ED spots distributed along the diffraction rings drawn for SnO_2 ; (c) EDXS spectrum showing strong Sn peaks but with evidence for the presence of O around the selected area; (d) TEM image of another Sn particle; (e) selected area ED spots of zone [331] or distributed along the diffraction rings drawn for Sn; and (f) EDXS spectrum showing strong Sn peaks and lower O content around this selected area.

eutectic SnAg solder foil following the reflow process RP2. The effective bonding areas on both sides occupy approximately 40% of the total contact area between the Sn coating and the SnAg solder foil as seen in Fig. 9(b). Some voids still remain between the Sn coating and the SnAg solder foil. They are probably associated with the tin oxide left at the valleys of the rough coating surface following abrading with SiC.

After the flux reflow process RP3 (carried out in air), the Sn coating had de-bonded from the Al substrate, Fig. 9(c). This can be understood because Al reacts rapidly with oxygen in air to form a thin oxide scale. Although the flux was successful in removing the tin oxide from the Sn coating surface, it failed to prevent the Al substrate forming this

thin layer of oxide on its surface. As a result of the gradual spreading of the alumina along the coating/Al interface, the molten Sn was displaced from the Al substrate. Most of the molten Sn coating coalesced with the molten SnAg solder (not visible in Fig. 9(c)). A few non-wetting isolated Sn droplets remain attached to the roughened surface of the Al substrate (previously the coating/Al interface).

3.2.2. Sn coating on Cu substrate – coating AC1

After reflow process RP1 under nitrogen, the Sn coatings on the two sides of the DBC/Sn–Sn/DBC sample were not joined together (see Fig. 3(b) for schematic of process). Again, this can be attributed to tin oxide on the coating surface. Intermetallic compounds (IMCs),

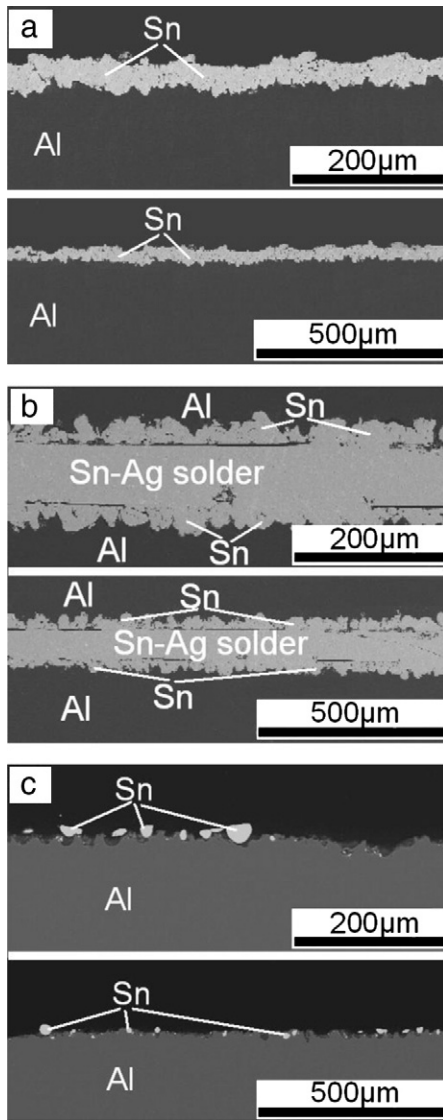


Fig. 9. SEM images of the polished cross-sections of the Al/Sn-SnAg-Sn/Al (AA1) samples following different reflow processes: (a) RP1; (b) RP2; and (c) RP3.

possibly Cu_6Sn_5 and/or Cu_3Sn , were also found to form between the Sn coating and the Cu substrate (Fig. 10(a)). This reveals that a metallurgical interfacial reaction occurred during the reflow process. Therefore, the oxides on both the Cu substrate and the Sn powder particles were presumably broken down during cold spraying and the Sn coating had intimate contact with the Cu surface. Unlike the surface profile of the Sn coating on the Al substrate, the surface profile of the Sn coating on the Cu substrate is seen to have changed significantly after the reflow process RP1. This might be related to the modification of flowability of the molten Sn due to the formation of the IMCs at the interface. Alternatively, the surface profile of the thinner Sn coating on the Cu substrate should be more stable than that of the thicker Sn coating on the Al substrate.

After abrading using SiC paper and then subjecting the joint to reflow process RP2, the Sn coating on the two sides of the DBC/Sn-Sn/DBC sample were locally joined together (Fig. 10(b)). Because the surface of the Sn coating on the Cu substrate is more irregular than the Sn coating on the Al substrate, more tin oxide may remain on the coating surface after the light abrading process. As a result, the ratio of the bonded area to the total contact area was lower than that achieved in the Al/Sn-SnAg-Sn/Al sample under an identical abrading and reflow process (Figs. 9(b) and 10(b)).

By contrast, after the flux reflow process RP3 in air, an effective solder joint was achieved as shown in Fig. 10(c) and (d). Thus, flux apparently removes the tin oxide on the surface during the reflow process and, in the case of the Cu substrate, oxidation of the substrate did not apparently occur and so Sn was able to wet the Cu substrate. The presence of pores and/or voids within the solder joint indicate that further process optimization is required.

For the reflow samples on the DBC substrate, the IMC layer between Sn and Cu was approximately 1 μm in thickness. EDX analysis of the IMC layer gave a composition of 66 at.% Cu and 34 at.% Sn (point A in Fig. 10(d)), or 64 at.% Cu and 36 at.% Sn (point B in Fig. 10(d)). However, because of the effect of electron beam spreading in the sample, this does not accurately reflect the composition of the IMC layer alone which is expected to be either Cu_6Sn_5 or Cu_3Sn .

4. Discussion

4.1. Cold spraying

During cold spraying, bonding is achieved mainly through adiabatic shear instabilities caused by high strain rate deformation due to the high-velocity impact of the powder particles [6]. According to theoretical investigations of cold spraying [5,6,11], at least three important velocities are associated with coating build up. The first one is the critical velocity that a powder particle must reach so that it can bond with the substrate surface. The second one is the critical velocity that is related to the self-bonding capability of the coating material so that a thick coating can be built up. The third one is the velocity above which few coating particles will adhere to either the surface of the substrate or previously deposited coating material and instead will cause erosion. These three important velocities all decrease with increasing particle size and temperature [5,6]. There is also a minimum particle diameter to allow a localized adiabatic shear instability to occur at the surface of an impacting particle. Schmidt et al. [6] have estimated a value of around 9 μm for a Sn particle based on certain approximations relating to characteristic length for thermal diffusion and critical velocity for impact. However, the latter is difficult to predict and depends on a number of factors. Nonetheless, a particle whose size is smaller than a diameter of this order would not achieve a shear instability necessary for bonding.

Overall, the impact velocity of a Sn powder particle is expected to increase with the pressure of the helium gas and the impact velocity of a larger Sn particle is lower than that of a smaller Sn particle under an identical gas pressure. Thus for the coatings AA2 formed on Al substrate using a higher gas pressure, the Sn particles can be assumed to have higher impact velocities and thus relatively larger Sn particles are expected to bond with the substrate. This would result in deeper and larger craters on the original surface of the substrate as is observed in the present work. This is the reason why the coating/substrate interface is more irregular in AA2 than the coating/substrate interface of AA1, produced using a lower pressure of the helium gas. On the other hand, it is also more likely for smaller Sn particles to reach the erosion velocity. As a result, the coating AA2 is discontinuous and has an average thickness slightly smaller than the coating AA1.

For the coating AC1, deposited on the relatively harder Cu substrate, the size of the Sn particle which reached the first critical velocity is smaller than for the coating AA1. Consequently, fewer and smaller Sn particles may well have been deposited on the initial surface of the Cu substrate. The average thickness of this coating is thus somewhat lower, and the coating/substrate interface consisting of the impact craters is somewhat smoother than the coating AA1. However, the surface of the coating AC1 appears to be more irregular and the reasons for this are not clear.

From the above discussion, it can be seen that only Sn particles within a relatively narrow size range can be effectively deposited. Those outside this range, both smaller and larger, would not have

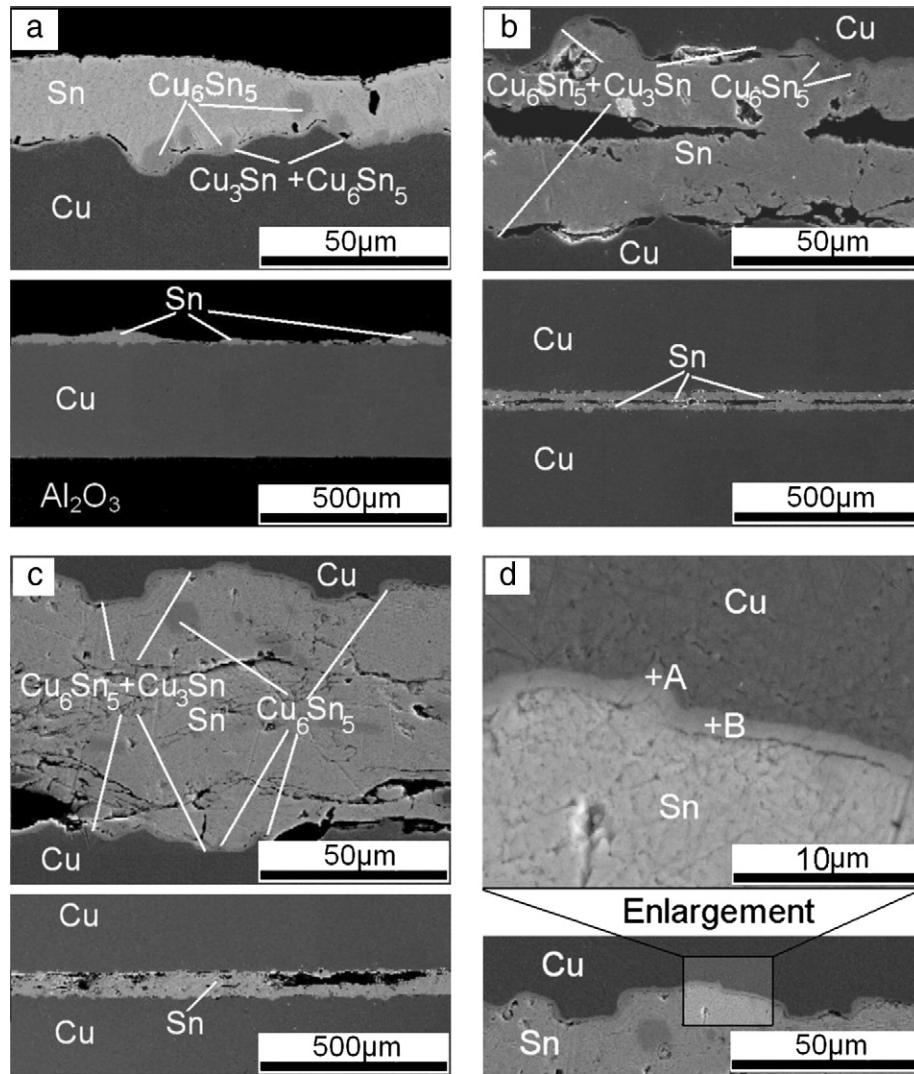


Fig. 10. SEM images of the polished cross-sections of the DBC/Sn-Sn/DBC (AC1) samples following different reflow processes: (a) RP1; (b) RP2; (c) RP3. (d) is higher magnification images of the sample following reflow process RP3, showing the morphology of the intermetallic (IMC) layer.

been deposited and this could be why the coating thickness variations all follow a normal distribution even though the feedstock powder has a multi-mode distribution as shown in Fig. 1. During cold spraying, the coating AA2 suffered stronger erosion whilst also being formed from the deposition of larger Sn particles than the coating AA1 as a result of the higher particle velocities. Thus the thickness variation of the AA2 coating is seen to have more scatter than that of the AA1 coating.

The deposition efficiencies of the Sn coatings achieved in the present work are clearly higher than the deposition efficiency of 5% for cold sprayed Sn on steel substrates reported by Legoux et al. [11]. This could be attributed to the following two facts. First, Al and Cu substrates were used that are softer than steel. Secondly, a lower pressure of the driving helium gas was used which probably resulted in lower particle velocities than in Ref. [11]. Although the impact velocities were not measured, a certain proportion of the Sn particles must have achieved the impact velocities between the second critical velocity and the erosion velocity. In Legoux et al.'s investigation [11], the impact velocities of the Sn particles were thought to be already higher than the erosion velocity. In addition, as aforementioned, a second spray pass led to the de-bonding of the deposited Sn coatings. This could be attributed to the accumulation of residual stress and stored elastic energy with increasing thickness of the coating. Nevertheless, it should be possible to build thicker Sn coatings using the present spraying conditions if the residual stress can be controlled.

The de-bonded coatings produced using two passes were almost four times the thickness of those produced using a single pass. This may be due to the fact that more particles contributed to roughening the substrate surfaces and/or were difficult to deposit on the previously relatively smooth surfaces during the first pass. As was also reported by Legoux et al. [11], many Sn particles can be deposited on a sandblasted surface but none was found to bond on to the polished surface of a steel substrate.

In Ning et al.'s work on cold sprayed Al-Sn coatings on Al6061, copper and SUS 304 substrates, melting of the tin phase was reported [14]. However, this is not the case for the present Sn coatings deposited on both Al and Cu substrates. If the melting of Sn had occurred, Cu_6Sn_5 intermetallic would have been observed at the coating/Cu interface of the as-sprayed Sn coating AC1. This is because the formation of Cu_6Sn_5 IMC was found to be almost instantaneous once fresh Cu was put in contact with liquid Sn [25].

4.2. Solderability

According to the Al-Sn binary phase diagram, an IMC does not form between Al and Sn [26]. The mechanical bonding between the cold sprayed Sn coating and the Al substrate was seen to be stable after the reflow process under nitrogen (RP1 and RP2). If the surface oxide on the Sn coating can be avoided or effectively removed, cold

sprayed Sn coatings in combination with a reflow process under vacuum and/or inert environment could provide an opportunity to solder Al or Al alloy components together. As presented in the results, the surface oxide came from the as-received Sn powder, rather than being produced during the cold spraying process. However, the use of flux under air led to de-bonding of the sprayed Sn coating from the Al substrate (RP3). Therefore, suitable approaches have to be investigated for the effective removal of the surface oxide without damaging the bonding between the coating and the aluminium substrate. Possible approaches include plasma cleaning of the sprayed Sn coatings or use of ultrasonic scrubbing during the reflow process to break down the surface oxide.

The problem associated with the surface oxide also existed for the soldering of the Sn coating on the DBC substrate under the fluxless reflow conditions. However, this problem was resolved using the flux-supported reflow process in air. Given that some pores or voids normally exist in conventional solder joints, the quality of the Cu/Sn/Cu solder joint achieved using the cold sprayed Sn coating as the solder layer under the flux-supported reflow condition has the potential to be acceptable for applications in electronic packaging and interconnects. Strong fluxes may be further investigated to reduce the pores or voids within the solder joints.

Generally speaking, the surface roughness needs to be considerably less than the coating thickness to ensure uniformity of the resulting solder thickness and reduce the possibility of voiding. A rougher surface might also result in poor wetting especially for fluxless processes. The surface roughening of the substrate should be also noted when considering cold spraying to deposit Sn layers for soldering in electronic packaging and interconnects. As described by the results of roughness analysis, the surface of any substrate used for deposition of a Sn layer has roughness parameters R_p and R_v , close to 20 μm for the Al substrate, and close to 10 μm for the Cu substrate (Table 3). They are generally the result of surface activation for the substrate subjected to impact of the feedstock powder particles. The contact metallization layers, e.g. Cu or Ni, on semiconductor devices are generally thinner than this, of the order of 5 μm . With this consideration, Sn coatings can be deposited on the supporting substrate, base-plate or heat sink, but not on the semiconductor devices. However, it could be possible to reduce the surface roughness of the substrate to some extent by using a finer particle size.

5. Conclusions

Sn powder has been successfully deposited by a single cold spray pass onto pure Al and DBC substrates.

The roughness of the coating/substrate interface depended on the type of substrate employed but this was not the case for the surface roughness of the coating.

SnO_2 was found on the surface of feedstock powder and also on the surfaces of the cold sprayed Sn coatings.

Using solder reflow process conditions referred to as RP1, a solder bond did not form with either Al or DBC substrate samples.

Following an otherwise identical procedure as RP1 but lightly abrading the Sn surface (reflow process RP2), bonding was improved. In the case of the Al substrate bonding increased with a Sn–Ag solder interlayer and with the DBC substrate direct bonding between cold sprayed layers was observed.

An effective solder joint was achieved with a flux enhanced reflow process (termed RP3) in the case of the DBC substrate but not with the Al substrate.

IMCs formed during the soldering trials of DBC substrates, demonstrate that a metallurgically clean Sn/Cu interface was obtained by cold spray deposition of Sn onto Cu.

Acknowledgements

This research was funded by the Engineering and Physical Sciences Research Council and the Innovative Electronic Manufacturing Research Centre in the UK.

References

- [1] A.P. Alkhimov, V.F. Kosarev, A.N. Papyrin, *Sov. Phys. Dokl.* 35 (1990) 1047.
- [2] R.C. Dykhuizen, M.F. Smith, *J. Therm. Spray Technol.* 7 (2) (1998) 205.
- [3] T. Stoltenhoff, H. Kreye, H.J. Richter, *J. Therm. Spray Technol.* 11 (4) (2002) 542.
- [4] D. Zhang, P.H. Shipway, D.G. McCartney, *J. Therm. Spray Technol.* 14 (1) (2005) 109.
- [5] T. Schmidt, F. Gaertner, H. Kreye, *J. Therm. Spray Technol.* 15 (4) (2006) 488.
- [6] T. Schmidt, F. Gaertner, H. Assadi, H. Kreye, *Acta Mater.* 54 (2006) 729.
- [7] F. Gaertner, T. Schmidt, H. Kreye, *Mater. Sci. Forum* 534–536 (2007) 433.
- [8] M. Fukumoto, H. Wada, K. Tanabe, M. Yamada, E. Yamaguchi, A. Niwa, M. Sugimoto, M. Izawa, *J. Therm. Spray Technol.* 16 (5–6) (2007) 643.
- [9] P.S. Phani, D.S. Rao, S.V. Joshi, G. Sundararajan, *J. Therm. Spray Technol.* 16 (3) (2007) 425.
- [10] J. Vlcek, L. Gimeno, H. Huber, E. Lugscheider, *J. Therm. Spray Technol.* 14 (1) (2005) 125.
- [11] J.G. Legoux, E. Irissou, C. Moreau, *J. Therm. Spray Technol.* 16 (5–6) (2007) 619.
- [12] W.Y. Li, C.J. Li, H. Liao, C. Coddet, *Appl. Surf. Sci.* 253 (14) (2007) 5967.
- [13] X. Guo, G. Zhang, W.Y. Li, L. Dembinski, Y. Gao, H. Liao, C. Coddet, *Appl. Surf. Sci.* 254 (5) (2007) 1482.
- [14] X.J. Ning, J.H. Jang, H.J. Kim, C.J. Li, C. Lee, *Surf. Coat. Technol.* 202 (9) (2008) 1681.
- [15] S. Marx, A. Paul, A. Koehler, G. Huettl, *J. Therm. Spray Technol.* 15 (2) (2006) 177.
- [16] E. Calla, *Cold Gas Spraying of Copper and Tin onto Metallic and Non Metallic Substrates*, Ph. D. Thesis of the University of Nottingham (2005).
- [17] B.A. Gillispie, Z. Zhao, J. Robert, H. Van Thomas, Y. Luo, H.F. Hutchins, *Product and method of brazing using kinetic – sprayed coatings*, US Patent 6 949 300 B2 (2005).
- [18] T.H. Van Steenkiste, J.R. Smith, R.E. Teets, J.J. Moleski, D.W. Gorkiewicz, R.P. Tison, D.R. Marantz, K.A. Kowalsky, W.L. Riggs, P.H. Zajchowski, B. Pilsner, R.C. McCune, K.J. Barnett, *Surf. Coat. Technol.* 111 (1) (1999) 62.
- [19] G. Humpston, D.M. Jacobson, *Principles of Soldering*, ASM International, Materials Park, Ohio 44073-0002, 2004.
- [20] D.D.L. Chung, *Appl. Therm. Eng.* 21 (2001) 1593.
- [21] C.K. Lin, C.C. Berndt, *J. Mater. Sci.* 30 (1995) 111.
- [22] J.F. Li, C.X. Ding, *J. Mater. Sci. Lett.* 18 (1999) 1591.
- [23] S. Guessasma, G. Montavon, C. Coddet, *Surf. Coat. Technol.* 173 (2003) 24.
- [24] W.K. Choi, J.S. Cho, S.K. Song, H.J. Jung, S.K. Koh, *Jpn. J. Appl. Phys.* 35 (1996) 5820.
- [25] T. Laurila, V. Vuorinen, J.K. Kivilahti, *Mater. Sci. Eng. R.* 49 (2005) 1.
- [26] Al–Sn phase diagram, http://www.crct.polymtl.ca/FACT/phase_diagram.php?file=Al-Sn.jpg&dir=SGTE.